Supporting Information

Tunable Subradiant Mode in Free-Standing Metallic Nanohole Arrays for High-Performance Plasmofluidic Sensing

Anran Li,[†] Xiaotian Wang,*[,†] Lin Guo,*[,†] Shuzhou Li*[,‡]

[†]Beijing Advanced Innovation Center for Biomedical Engineering, School of Chemistry, Beihang University, Beijing 100191, Beijing, P. R. China.

[‡]School of Materials Science and Engineering, Nanyang Technological University, Singapore 639798, Singapore.

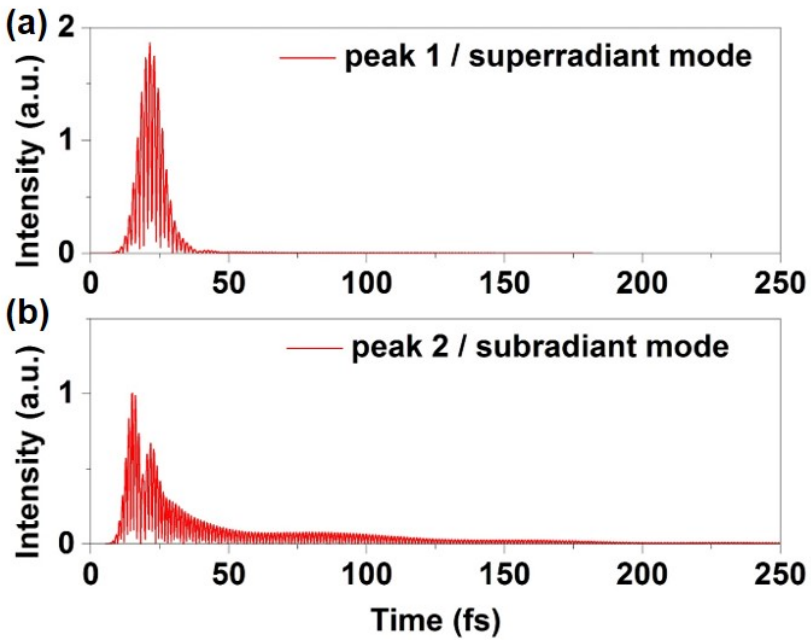

Figure S1. Temporal evolutions of the simulated electric field intensity for the peak 1/superradiant (a) and peak 2/subradiant (b) modes of the free-standing Ag hexagonal NA (p= 580 nm, r=180 nm, t= 100nm).

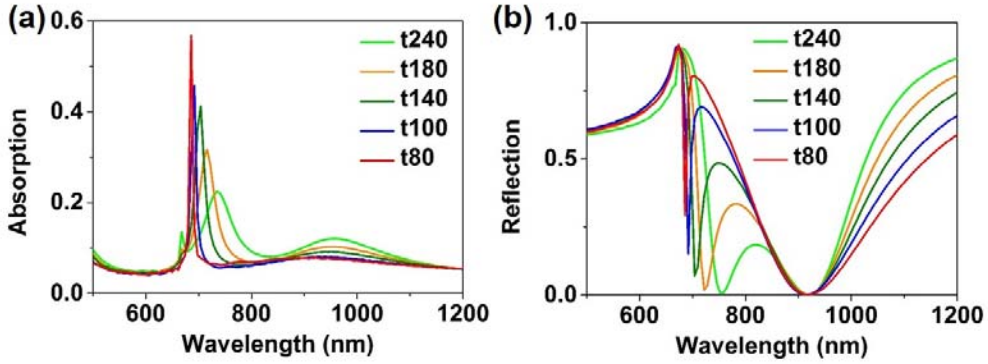

Figure S2. Absorption (a) and reflection (b) spectra of the free-standing Ag hexagonal NAs (p= 580 nm, r=180 nm) with various film thicknesses t.

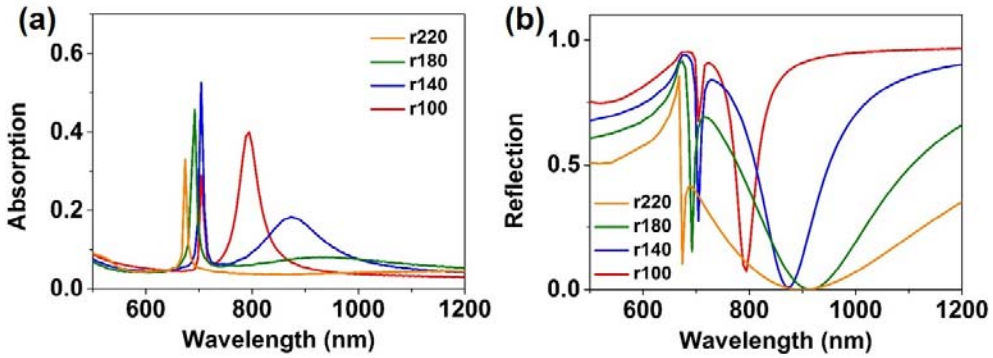

Figure S3. Absorption (a) and reflection (b) spectra of the free-standing Ag hexagonal NAs (p=580 nm, t=100 nm) with various hole sizes r.

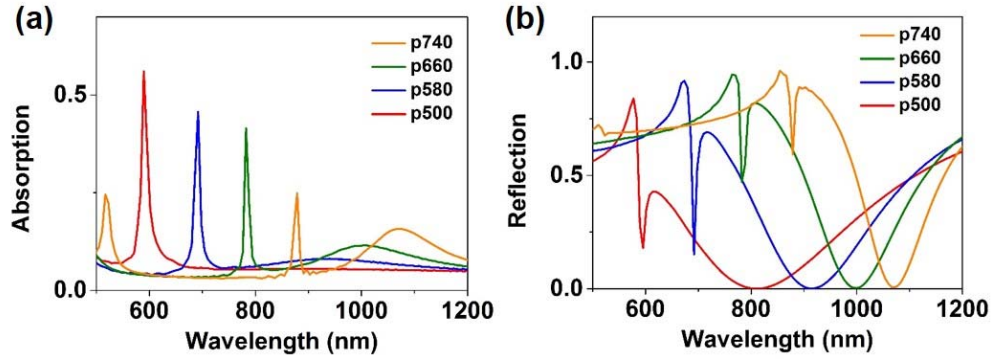

Figure S4. Absorption (a) and reflection (b) spectra of the free-standing Ag hexagonal NAs (t=100 nm, r=180 nm) with various periodicities p.

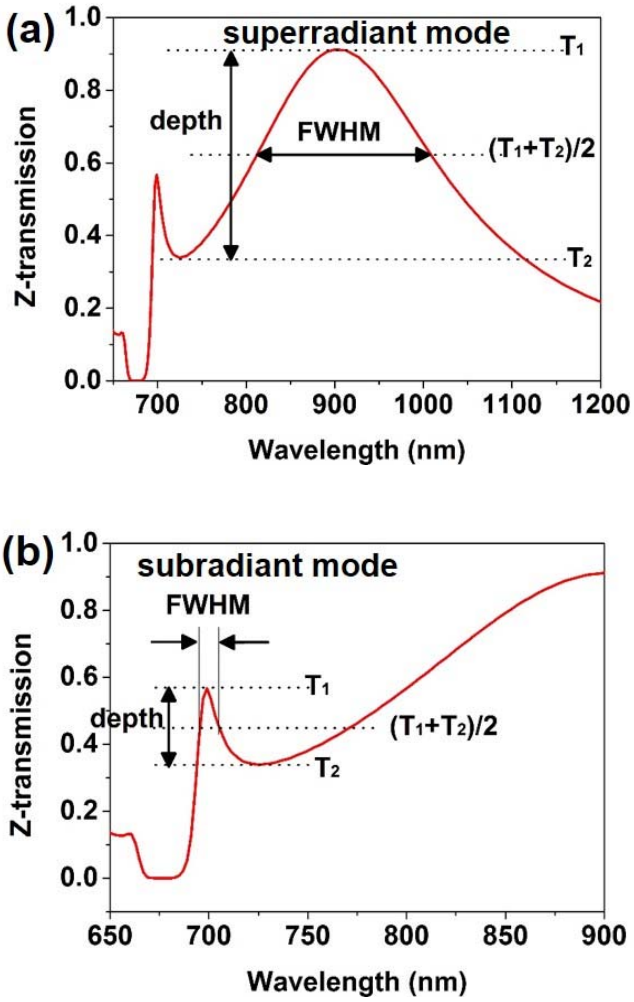

Figure S5. Determination of the FWHM and depth of the superradiant mode (a) and the subradiant mode (b).

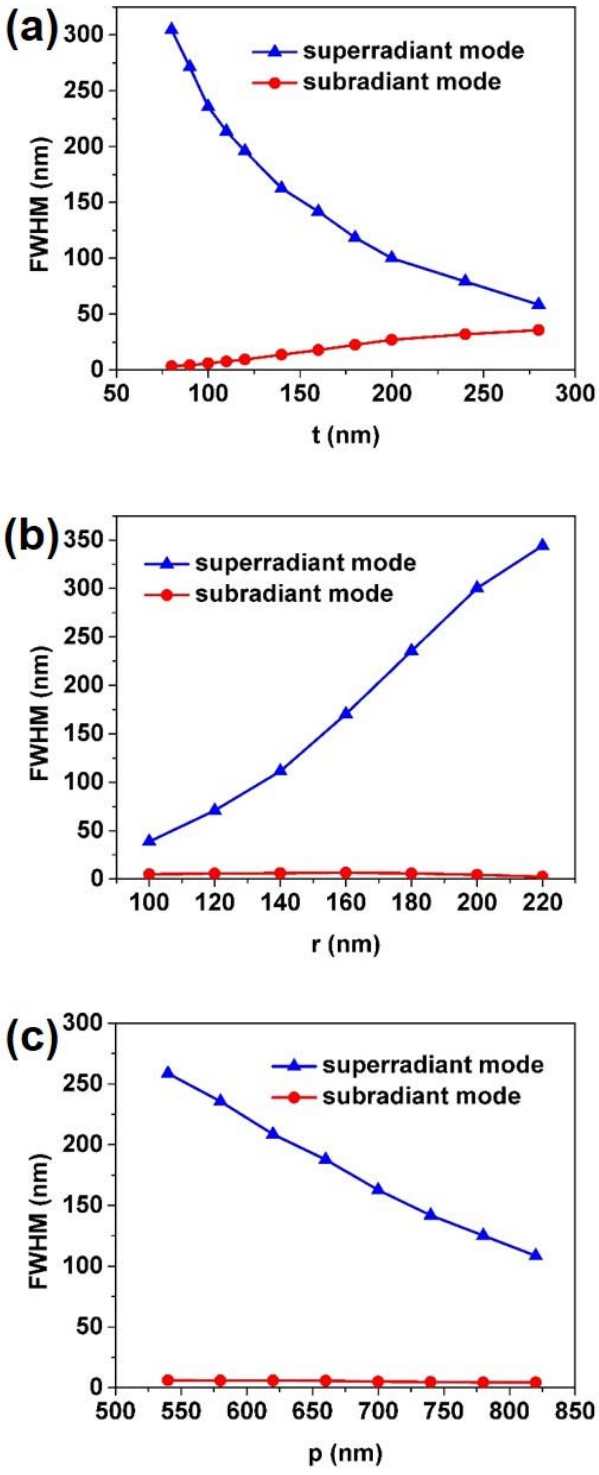

Figure S6. FWHM of the superradiant mode and the subradiant mode in free-standing Ag NAs as a function of (a) film thickness t (p=580 nm, r=180 nm), (b) hole radius r (p=580 nm, t=100 nm), and (c) lattice periodicity p (t=100 nm, r=180 nm).

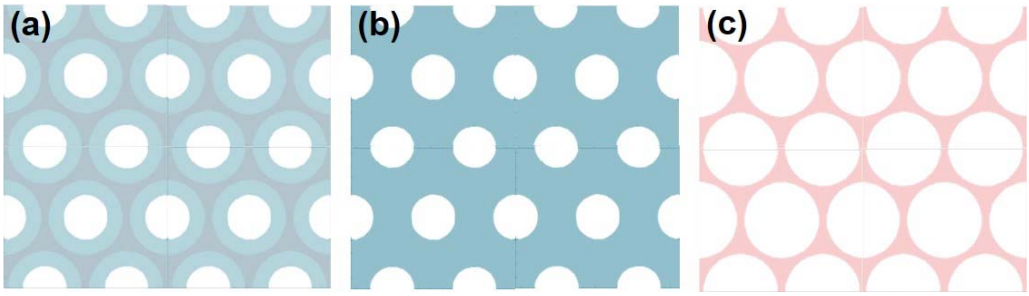

Figure S7. Schematic illustrations of the top views of (a) silver NAs placed on top of a free-standing SiO_2 membrane with through holes, (b) silver NAs, and (c) SiO_2 membrane with through holes.